nature structural & molecular biology

BTG4 is a meiotic cell cycle–coupled maternal-zygotic-transition licensing factor in oocytes

Chao Yu[1,5], Shu-Yan Ji[1,5], Qian-Qian Sha[1,5], Yujiao Dang[2,5], Jian-Jie Zhou[1,5], Yin-Li Zhang[1,5], Yang Liu[1], Zhong-Wei Wang[3], Boqiang Hu[2], Qing-Yuan Sun[3], Shao-Chen Sun[4], Fuchou Tang[2] & Heng-Yu Fan[1]

The mRNAs stored in oocytes undergo general decay during the maternal-zygotic transition (MZT), and their stability is tightly interconnected with meiotic cell-cycle progression. However, the factors that trigger decay of maternal mRNA and couple this event to oocyte meiotic maturation remain elusive. Here, we identified B-cell translocation gene-4 (BTG4) as an MZT licensing factor in mice. BTG4 bridged CNOT7, a catalytic subunit of the CCR4–NOT deadenylase, to eIF4E, a key translation initiation factor, and facilitated decay of maternal mRNA. *Btg4*-null females produced morphologically normal oocytes but were infertile, owing to early developmental arrest. The intrinsic MAP kinase cascade in oocytes triggered translation of *Btg4* mRNA stored in fully grown oocytes by targeting the 3′ untranslated region, thereby coupling CCR4–NOT deadenylase–mediated decay of maternal mRNA with oocyte maturation and fertilization. This is a key step in oocyte cytoplasmic maturation that determines the developmental potential of mammalian embryos.

Remodeling a fertilized egg into a totipotent zygote is an important and complex cell-transformation event in biology. Maternal mRNAs, which are synthesized and stored during oocyte growth, serve as the maternal contribution and support early embryo development but undergo general decay after meiotic resumption; in contrast, the zygotic genome is transcriptionally activated only in later cell cycles[1,2]. This transition from a maternal to a zygotic mode of development is called the MZT. Understanding of the MZT in mammals is a cornerstone of assisted-reproduction technology, because a large proportion of *in vitro*–matured human oocytes are morphologically normal but demonstrate MZT defects after fertilization[3].

A limited number of maternal-effect genes that regulate MZT have been identified in mice: protein products of *Mater* (official symbol *Nlrp5*), *Floped* (official symbol *Ooep*), *Tle6* (transducin-like enhancer of split 6), and *Filia* (official symbol *Khdc3*) form a maternal complex in the subcortexes of oocytes and embryos[4]; the product of *Hsf1* (heat-shock factor 1) is a major transactivator of stress-induced genes[5]; the product of *Npm2* (nucleoplasmin 2) is vital for nucleolar organization in early embryos[6]; *Zar1* (zygotic arrest 1) encodes an RNA-binding protein that regulates translation of other maternal mRNAs[7]. However, none of these genes directly regulate decay of maternal mRNA or zygotic genome activation (ZGA), which are the two core events of MZT. The key regulators of mammalian MZT remain elusive.

In mammals, oocyte meiotic maturation (i.e., the resumption of meiosis), a prologue to MZT, triggers a transition from mRNA stability to instability, thus suggesting the existence of an active mechanism triggering mRNA decay in oocytes[8]. Approximately 90% of maternal mRNAs are degraded by the two-cell stage in mouse embryos[9]. However, the mechanism that mediates activation of the mRNA-decay machinery during meiotic maturation and how this mechanism is coupled with meiotic cell-cycle progression are currently unclear. To answer these questions, we sought to investigate the *in vivo* function of *Btg4*, which is specifically expressed by mature oocytes. We identified *Btg4* as a meiotic cell cycle–coupled MZT licensing factor that triggers decay of maternal mRNA in maturing mammalian oocytes.

RESULTS

Btg4 knockout in mice causes female infertility

Previous transcriptome analyses have shown that *Btg4* mRNA is highly expressed in mouse and human oocytes[10,11], as we confirmed by quantitative RT–PCR (qRT–PCR; **Supplementary Fig. 1a**). The *Btg4* gene contains five exons and encodes a protein of 250 amino acids in mice (**Fig. 1a**). To study the physiological functions of *Btg4*, we generated a knockout mouse strain by using the transcription-activator-like effector nuclease (TALEN) system[12,13]. This strain contained a 7-nt deletion in exon 2 of the *Btg4* gene, which was disrupted with a ScaI site (**Fig. 1a**,**b** and **Supplementary Fig. 1b**). This deletion caused a reading-frame shift and created a premature stop codon. Western blotting analysis confirmed the presence of BTG4 proteins in the oocytes of these *Btg4*-null ($Btg4^{-/-}$) mice (**Fig. 1c**).

Although previous studies have shown that BTG and transducer of ErbB-2 (TOB) family proteins inhibit cell proliferation and might function as tumor suppressors[14,15], the $Btg4^{-/-}$ mice were viable and

[1]Life Sciences Institute and Innovation Center for Cell Signaling Network, Zhejiang University, Hangzhou, China. [2]Biodynamic Optical Imaging Center, College of Life Sciences, Peking University, Beijing, China. [3]State Key Laboratory of Reproductive Biology, Institute of Zoology, Chinese Academy of Sciences, Beijing, China. [4]College of Animal Science and Technology, Nanjing Agricultural University, Nanjing, China. [5]These authors contributed equally to this work. Correspondence should be addressed to H.-Y.F. (hyfan@zju.edu.cn).

Received 4 November 2015; accepted 11 March 2016; published online 11 April 2016; doi:10.1038/nsmb.3204

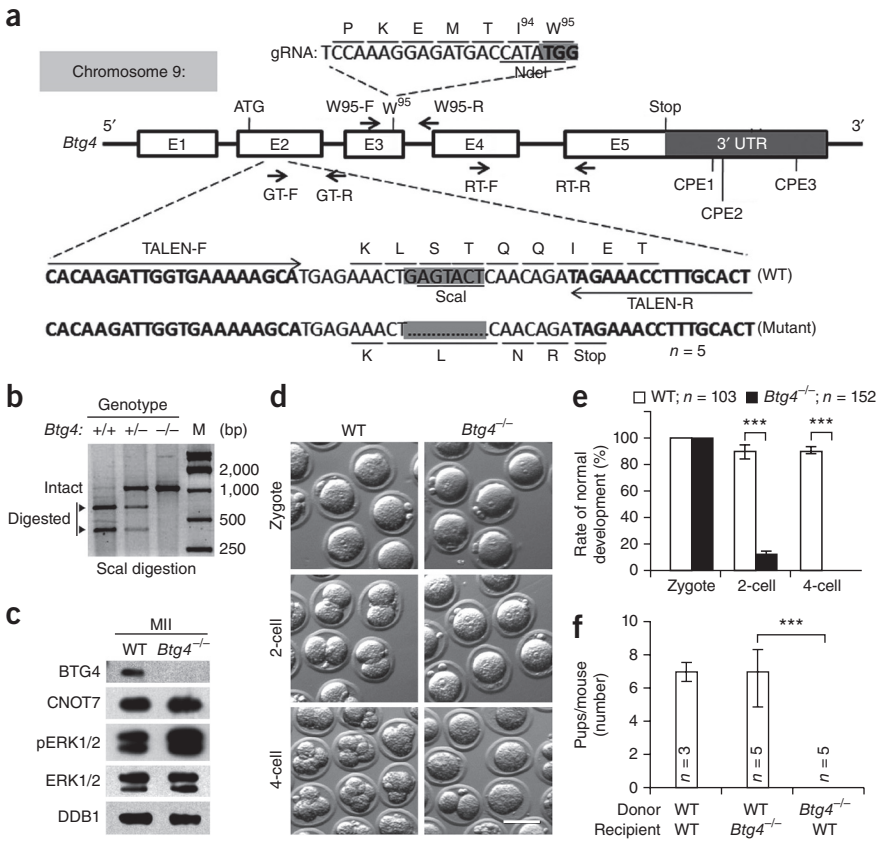

Figure 1 *Btg4* is a maternal-effect gene essential for MZT. (**a**) Gene-targeting strategy for *Btg4* knockout and *Btg4*^{W95A} knock-in alleles. F, forward; R, reverse; gRNA, guide RNA. (**b**) ScaI-digestion results of the PCR product amplified from the genomic DNA containing the TALEN targeting site. M, marker. (**c**) Western blot results showing BTG4 expression in oocytes of wild type (WT) and *Btg4*$^{-/-}$ females. Damaged DNA-binding protein-1 (DDB1) and ERK1/2 are protein loading controls; p, phospho. Uncropped western blot with molecular weight markers is shown in **Supplementary Data Set 1**. (**d**) Representative images of embryos derived from WT and *Btg4*$^{-/-}$ females. $n = 5$ mice for each genotype at different developmental stages. Scale bar, 50 μm. (**e**) Developmental rates of embryos collected from the oviducts of WT and *Btg4*$^{-/-}$ females. The number of embryos analyzed is indicated (*n*). Error bars, s.e.m. $^{***}P < 0.001$ by two-tailed Student's *t* test. (**f**) Average number of resulting pups from embryo transfers between donors and recipients, with indicated genotypes. The number of mice used is indicated (*n*). Error bars, s.e.m. $^{***}P < 0.001$ by two-tailed Student's *t* test.

had body sizes (**Supplementary Fig. 1c**) similar to those of their wild type (WT) littermates. They were healthy up to 1 year of age and did not spontaneously develop tumors. However, the *Btg4*$^{-/-}$ females were sterile, whereas the males exhibited normal fertility. *Btg4*$^{-/-}$ females displayed normal ovarian histology and ovulated metaphase II (MII) oocytes, and they underwent normal meiotic maturation *in vitro* (**Supplementary Fig. 1d–f**). However, some normally fertilized zygotes derived from *Btg4*$^{-/-}$ females developed to the two-cell stage (**Fig. 1d**,**e** and **Supplementary Fig. 1g**). We transferred WT zygotes into the oviducts of pseudopregnant *Btg4*$^{-/-}$ females (20 embryos per mouse) and conversely transferred *Btg4*$^{-/-}$ zygotes into WT females. The *Btg4*$^{-/-}$ females gave birth to WT pups with normal efficiency, but none of the embryos derived from *Btg4*$^{-/-}$ females developed to term in WT fosters (**Fig. 1f** and **Supplementary Fig. 1h**,**i**). To rule out the possibility of off-target effects, we also generated a clustered regularly interspaced short palindromic repeats (CRISPR) and CRISPR-associated protein 9 (CRISPR–CAS9)-directed *Btg4*$^{\Delta C/\Delta C}$ mouse strain in which the C-terminal 156 amino acids of BTG4 were truncated[16,17]. The *Btg4*$^{\Delta C/\Delta C}$ females were also infertile, and their embryos were arrested at the one- or two-cell stage (**Supplementary Fig. 1g**). The two independent mouse strains (*Btg4*$^{-/-}$ and *Btg4*$^{\Delta C/\Delta C}$) showed similar phenotypes. These results demonstrate that BTG4 is a new maternal factor that is crucial for MZT.

Impaired decay of maternal mRNA in oocytes of *Btg4*$^{-/-}$ females

WT and *Btg4*-deleted embryos exhibited similar levels of DNA-damage response, thus indicating that DNA damage did not underlie two-cell arrest (**Supplementary Fig. 2a**). We then investigated the key genome-reprogramming events in embryos of *Btg4*$^{-/-}$ mice. BTG4-deleted zygotes initiated DNA replication (as determined by 5-bromo-2-deoxyuridine incorporation; **Supplementary Fig. 2b**), converted 5-methylcytosine to 5-hydroxymethylcytosine in the male pronuclei (**Supplementary Fig. 2c**), and gained female-pronucleus-specific histone H3 trimethylation at Lys4 and Lys9 (**Supplementary Fig. 2d**,**e**). We detected markers of genome transcriptional activation—phosphorylated RNA polymerase II and acetylated histones (histone H2B Lys5, H3 Lys9, and H3 Lys18)—in embryos derived from both WT and *Btg4*$^{-/-}$ females (**Supplementary Fig. 3**).

We then investigated the effects of maternal *Btg4* deletion on mRNA metabolism during MZT. We subjected samples of oocytes at germinal vesicle (GV) and MII stages, zygotes, and two-cell embryos of both genotypes (WT and *Btg4*$^{-/-}$) to RNA-seq analyses, and the expression levels of genes were assessed as fragments per kilobase of transcript per million fragments sequenced (FPKM). We detected 11,453–13,106 genes (FPKM >0.1) from all samples (**Supplementary Fig. 4a** and **Supplementary Table 1**), and all replicates showed high correlations ($R \geq 0.909$; **Fig. 2a**). First, we analyzed the overall decay of maternal mRNA in WT and *Btg4*$^{-/-}$ oocytes during meiotic maturation and after fertilization by spiked-in exogenous GFP and RFP. As previously reported[18,19], 79% of mRNAs were degraded during meiotic maturation (GV to MII) in WT oocytes (**Fig. 2b**). Total mRNA was further decreased to 8% in zygotes. However, we observed a two-fold increase after the first mitosis (zygote to two-cell stage, from 8% to 17%), indicating early zygotic genome activation. In *Btg4*$^{-/-}$ oocytes, only 14% of mRNAs were degraded at the MII stage, and 64% and 67% were degraded at the one- and two-cell stages, respectively (**Fig. 2b**). These results suggest that decay of maternal mRNA was severely impaired in *Btg4*-knockout mice.

According to the expression patterns in WT oocytes and embryos, we divided transcripts into four clusters: cluster I, comprising transcripts that were substantially degraded at the GV–MII transition and did not subsequently reaccumulate in WT oocytes; cluster II, comprising transcripts that were markedly degraded after fertilization in WT oocytes; cluster III, comprising transcripts that were substantially upregulated at the zygote–two-cell transition (i.e., zygotic genes); and cluster IV, comprising transcripts that were markedly degraded at the GV–MII transition but reaccumulated at the zygote–two-cell

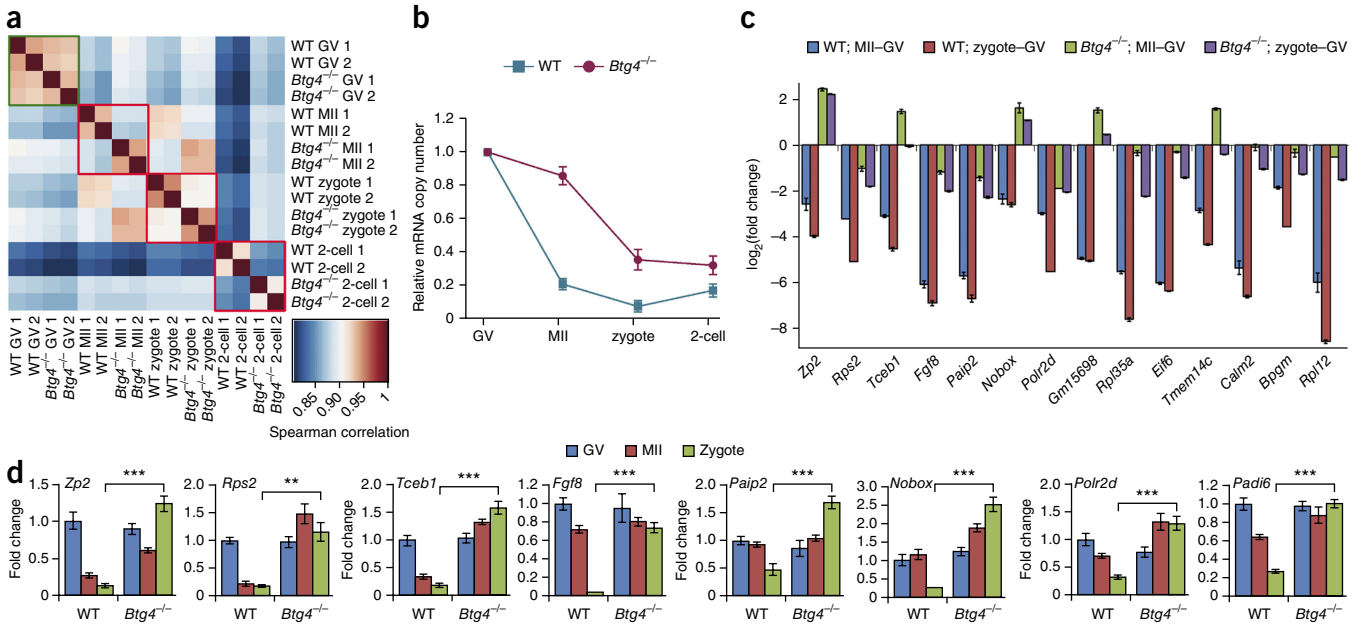

Figure 2 BTG4 is required for decay of maternal mRNA. (**a**) Heat map of Spearman correlation coefficients among WT and *Btg4*$^{-/-}$ oocytes and embryos at different stages. (**b**) Relative mRNA copy-number dynamics in WT and *Btg4*$^{-/-}$ samples at different stages. $n = 2$ embryo samples. Bars indicate range of values. (**c**) RNA-seq results showing the relative expression levels of representative genes. $n = 2$ embryo samples. Bars indicate range of values. (**d**) qRT–PCR showing the relative levels of the indicated transcripts in oocytes and zygotes of WT and *Btg4*$^{-/-}$ females. $n = 4$ technical replicates. Error bars, s.e.m. $^{**}P < 0.01$; $^{***}P < 0.001$ by two-tailed Student's *t* test.

transition (**Supplementary Fig. 4b–e**). We then compared the expression changes of these MZT-associated transcripts in WT and *Btg4*$^{-/-}$ oocytes and embryos. WT and *Btg4*$^{-/-}$ oocytes exhibited similar transcriptomes at the GV stage (**Fig. 2a** and **Supplementary Fig. 4b**). However, we found appreciable differences between the transcriptomes of WT and *Btg4*$^{-/-}$ oocytes and embryos at the later stages (**Fig. 2a**). More transcripts were upregulated than were downregulated in BTG4-deleted samples (fold change >2 or <0.5, $P < 0.05$, false discovery rate <0.05 by DESeq based on negative bionomial distribution model; **Supplementary Fig. 4b**). When overlapped with the transcripts that degraded during meiotic maturation and after fertilization (clusters I, II, and IV), 63.4% of these transcripts were not degraded in *Btg4*$^{-/-}$ MII oocytes and zygotes (**Supplementary Figs. 4d** and **5a**). Even at the two-cell stage, more maternal transcripts were upregulated than downregulated after BTG4 deletion (**Supplementary Fig. 5b**). These results suggest that BTG4 is crucial for the clearance of maternal mRNA. To account for the degradation of mRNAs in different samples (which varied from 8% to 100%), we normalized the FPKM values of genes to the corresponding FPKM values of GFP and RFP, performed RNA-seq (results for representative transcripts in **Fig. 2c**), and further confirmed the results by qRT–PCR (**Fig. 2d**). These maternal transcripts were degraded at MII and after fertilization but were not degraded in oocytes and zygotes of *Btg4*$^{-/-}$ females.

ZGA in *Btg4*$^{-/-}$ zygotes was also impaired. 5,854 transcripts were upregulated when WT zygotes developed to the two-cell stage, and most of these transcripts belonged to clusters III and IV (**Supplementary Fig. 4b**). However, in *Btg4*$^{-/-}$ two-cell embryos, many cluster III and IV transcripts were downregulated in comparison with those in WT two-cell embryos (**Supplementary Figs. 4e** and **5b**). Notably, more zygotic (cluster III) transcripts were downregulated than upregulated in two-cell embryos derived from *Btg4*$^{-/-}$ females (**Supplementary Fig. 5b**), thus suggesting impaired ZGA in *Btg4*$^{-/-}$ embryos (RNA-seq results for representative transcripts and qRT–PCR results in **Supplementary Fig. 5c,d**; sequences of PCR primers in **Supplementary Table 2**). Collectively, these results indicate that BTG4 triggers maternal mRNA clearance during oocyte maturation, which is a prerequisite for ZGA in mammals.

BTG4 stimulates 3′-poly(A)-tail shortening

In cytoplasmic mRNA turnover, deadenylation (shortening) of the poly(A) tail is the initial and often rate-limiting step[18]. For transcripts that were normally degraded during MZT but that were stabilized by BTG4 deletion, poly(A) tails were shortened in maturing WT oocytes, but this shortening was blocked or delayed in the oocytes and zygotes of *Btg4*$^{-/-}$ mice (**Fig. 3a,b**). These results indicate that BTG4 triggers decay of maternal mRNAs by mediating the deadenylation of their poly(A) tails.

BTG4 belongs to the BTG and TOB protein family, which has six members in vertebrates[14,19]. However, only BTG4 is expressed exclusively in human and mouse oocytes and early embryos (**Supplementary Figs. 1a** and **5e,f**). Except for BTG4, all BTG and TOB proteins have been reported to interact with CNOT7 and CNOT8, the catalytic subunits of the CCR4–NOT deadenylase[20–23]. *Cnot7* and *Cnot8* mRNAs were highly expressed in mouse oocytes and embryos (**Supplementary Fig. 5g,h**). Coimmunoprecipitation (Co-IP) experiments showed that BTG4 interacted with CNOT7 and CNOT8 (**Fig. 3c,d**). Consistently with previous structural insights[24], many conserved amino acid residues in the BTG domain were required for BTG4-CNOT7 interactions (**Fig. 3c**). Among these, the BTG4^{W95A} mutant abolished the BTG4-CNOT7 and BTG4-CNOT8 interactions (**Fig. 3c,d**). The conserved K203 residue in CNOT7 was also essential for BTG4-CNOT7 binding (**Fig. 3e**).

To determine whether BTG4 functions through the CCR4–NOT deadenylase *in vivo*, we generated a *Btg4*^{W95A} knock-in mouse strain by using the CRISPR–CAS9 system (**Figs. 1a** and **4a**) and crossed these mice with *Btg4*-null mice to obtain *Btg4*$^{W95A/-}$ females. BTG4^{W95A} proteins were expressed in the *Btg4*$^{W95A/-}$ oocytes (**Fig. 4b**). However, *Btg4*$^{W95A/-}$ female mice were infertile, and their

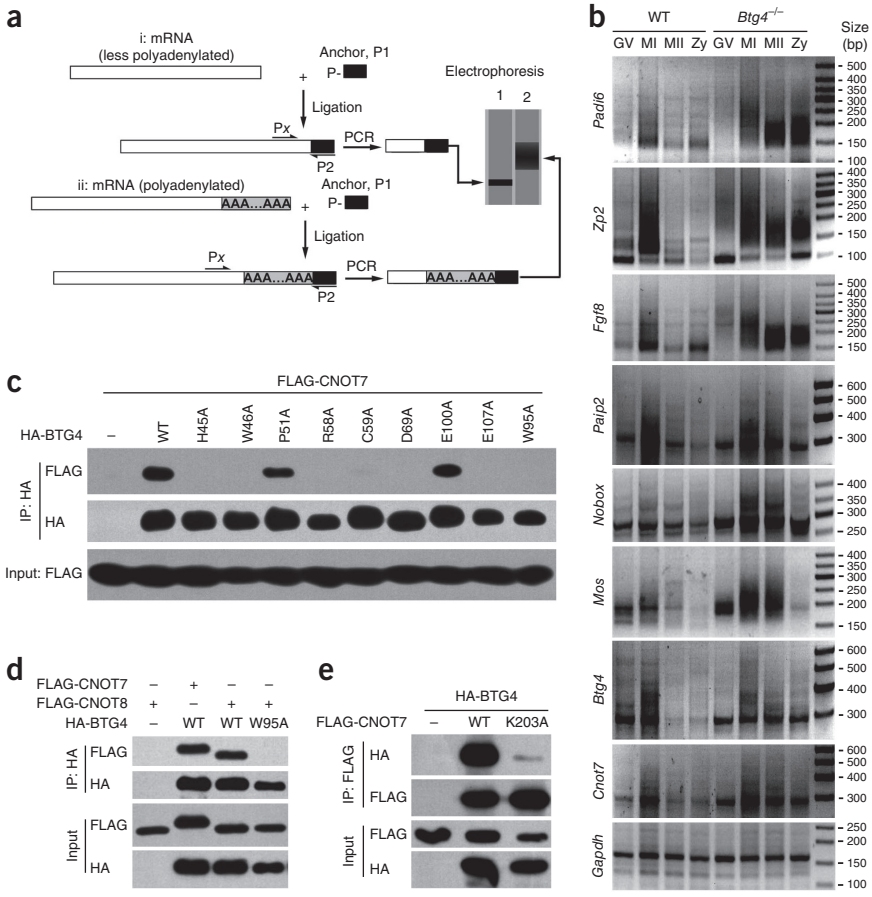

Figure 3 BTG4 interacts with CCR4–NOT transcription-complex subunits CNOT7 and CNOT8 and is required for 3′-poly(A)-tail shortening of maternal transcripts. (**a**) Diagram showing the strategy of the mRNA poly(A) tail (PAT) assay. P1, anchor primer; P2, P1-antisense primer; P*x*, gene-specific primer. (**b**) PAT assay results showing changes in poly(A)-tail length for the indicated transcripts in oocytes and zygotes collected from WT and *Btg4*$^{-/-}$ females. Zy, zygote. (**c**,**d**) Identification of conserved amino acid residues that are essential for BTG4-CNOT7 (**c**) and BTG4-CNOT8 (**d**) interaction. (**e**) Immunoprecipitation and western blot results showing the interaction between BTG4 and CNOT7. HA, hemagglutinin tag. Uncropped images for western blots are in **Supplementary Data Set 1**.

phenotypes mimicked those of *Btg4*$^{-/-}$ mice because their fertilized oocytes were arrested at the one- or two-cell stage (**Fig. 4c**,**d**). In addition, the maternal transcripts that were degraded during normal oocyte maturation were stabilized in *Btg4*$^{W95A/-}$ oocytes and zygotes (**Fig. 4e**). These results provide *in vivo* evidence that BTG4 functions through the CCR4–NOT deadenylase in triggering decay of maternal mRNA during MZT.

BTG4 recruits CNOT7 to eIF4E–mRNA complexes

In an *in vitro* deadenylation assay, BTG4 binding did not affect the RNA deadenylase activity of CNOT7 (**Supplementary Fig. 6a**). Previous studies have suggested that BTG proteins might function as adaptors in recruiting mRNAs to CCR4–NOT deadenylase[21,25]. eIF4E is potentially involved in mRNA decay, because it has been reported to interact with ANGEL1, a member of the CCR4 deadenylase family[26]. We found that endogenous BTG4 bound to CNOT7 as well as to eukaryotic translation initiation factor 4E (eIF4E) in mature mouse oocytes (**Fig. 5a**). Ectopically expressed BTG4 in HeLa cells also bound to eIF4E independently of CNOT7, because the mutation of W95 in BTG4 did not affect BTG4-eIF4E binding (**Fig. 5b**). Moreover, purified eIF4E and CNOT7 proteins directly interacted with *Escherichia coli*–expressed BTG4 protein in cell-free buffers (**Fig. 5c**). A further binding assay using truncated BTG4 showed that boxB was crucial for BTG4-eIF4E interaction (**Fig. 5d**). BTG2 and BTG3 also bound to eIF4E through boxB within their BTG domains (**Supplementary Fig. 6b**,**c**), thus suggesting that eIF4E-binding ability is shared by all BTG family members. However, eIF4E's C-terminal domain interacted with BTG4 (**Supplementary Fig. 6d**,**e**); this domain is required for binding to eIF4G and the 5′-cap of mRNA[27–29].

We further determined whether BTG4 mediated the interaction between eIF4E and CNOT7. In HeLa cell lysates, we detected weak binding between CNOT7 and eIF4E, but this binding was further weakened by the CNOT7^{K203A} mutation, which abolished CNOT7-BTG binding, thus suggesting that the CNOT7-eIF4E interaction is mediated by endogenous BTG proteins (**Fig. 5e**). BTG4 overexpression increased the eIF4E binding efficiency of CNOT7^{WT} but not CNOT7^{K203A} (**Fig. 5e**). In contrast, overexpression of BTG4^{W95A}, which bound eIF4E but not CNOT7, decreased the efficiency of CNOT7-eIF4E interaction in a dominant-negative manner (**Fig. 5f**). Degradation of maternal mRNA was also impaired after *Eif4e* depletion (**Fig. 5g**,**h**). These results suggest that BTG4 functions as an adaptor that recruits CNOT7 to eIF4E. By this mechanism, the CCR4–NOT complex is recruited to the actively translating mRNA in oocytes and zygotes.

ERK1/2 couples *Btg4* translation to oocyte maturation

Although *Btg4* and *Cnot7* mRNA levels were high in GV oocytes, we detected expression of the corresponding proteins only after GV breakdown; this expression reached a maximal level at the MII stage and quickly decreased after the two-cell stage (**Fig. 6a**,**b**; anti-BTG4 and anti-CNOT7 antibody information in **Supplementary Table 3**). In oocytes injected with mRNAs encoding GFP-BTG4, GFP-BTG4 was expressed in GV and MII oocytes at comparable levels, but endogenous BTG4 was present in only MII oocytes (**Supplementary Fig. 7a**,**b**). These results indicate that *Btg4*-mRNA translation, rather than BTG4 protein stability, is coupled to meiotic maturation.

Next, we sought to determine the signal that coupled BTG4 accumulation to oocyte meiotic maturation. The poly(A) tail of *Btg4* mRNA remained short at the GV stage and was elongated after meiotic resumption but was quickly shortened at MII (**Fig. 3b**). The mouse *Btg4* mRNA has a 347-bp 3′ untranslated region (UTR), which contains three putative cytoplasmic polyadenylation elements (CPEs) (**Fig. 1a**). We cloned the mouse *Btg4* 3′ UTR, fused it with FLAG-GFP, *in vitro*–transcribed the construct, and injected it into GV oocytes along with mRNA encoding mCherry. After 14 h, we detected GFP signals in MII- but not in GV-arrested oocytes, whereas we found that mCherry was equally expressed in GV and MII oocytes (**Fig. 6c**,**d** and **Supplementary Fig. 7c**). Furthermore, all three CPEs in the *Btg4* 3′ UTR contributed to mRNA translation in

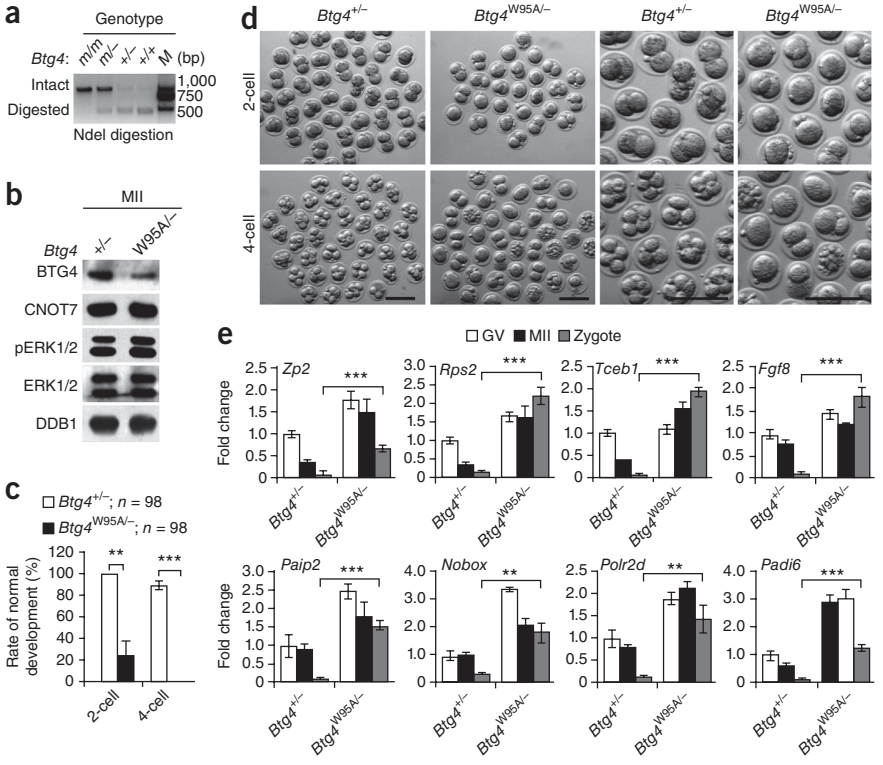

Figure 4 Interaction with CNOT7 and CNOT8 is essential for BTG4 function *in vivo*. (**a**) NdeI-digestion results of the PCR product amplified from the genomic DNA containing the *Btg4*^{W95} site. m, *Btg4*^{W95A}. (**b**) Western blot result showing the expression levels of the indicated proteins in MII oocytes of *Btg4*$^{+/-}$ and *Btg4*$^{W95A/-}$ females. Uncropped images are in **Supplementary Data Set 1**. (**c**) Developmental rates of embryos from *Btg4*$^{+/-}$ and *Btg4*$^{W95A/-}$ knock-in females. The number of embryos analyzed is indicated ($n = 98$ embryos). Error bars, s.e.m. $^{**}P < 0.01$; $^{***}P < 0.001$ by two-tailed Student's *t* test. (**d**) Representative images of embryos derived from WT and *Btg4*^{W95A} knock-in females. $n = 5$ mice for each genotype at each time point. Scale bars, 100 µm. (**e**) qRT–PCR showing the relative levels of indicated transcripts in oocytes and zygotes of *Btg4*$^{+/-}$ and *Btg4*$^{W95A/-}$ females. $n = 4$ technical replicates. Error bars, s.e.m. $^{**}P < 0.01$; $^{***}P < 0.001$ by two-tailed Student's *t* test.

an additive manner (**Fig. 6c**,**d**). Interestingly, adding poly(A) tails to *in vitro*–transcribed FLAG-GFP–*Btg4* 3′-UTR mRNAs or the CPE-mutated version uncoupled the expression with the meiotic cell cycle, and we detected ectopic GFP signals in GV-arrested oocytes (**Supplementary Fig. 7d**). These results indicated that CPE-mediated polyadenylation is a necessary and rate-limiting step of *Btg4*-mRNA translation.

In *Xenopus* oocytes, aurora A kinase–mediated phosphorylation of cytoplasmic polyadenylation element binding protein-1 (CPEB1) is essential for the translation of many maternal transcripts[30–32]. Short interfering RNA–mediated *Cpeb1* depletion blocked BTG4 expression (**Fig. 6e**) and impaired PB1 emission and meiotic-spindle assembly (**Supplementary Fig. 8a–d**), as previously reported[33,34]. However, MLN8237, an inhibitor of aurora A, blocked PB1 emission and impaired chromosome separation but did not affect BTG4 expression (**Supplementary Fig. 8e–h**). These results indicate that although CPEB1 is required for BTG4 expression, it is activated by an aurora A–independent mechanism in mouse oocytes.

Mitogen-activated protein kinase (MAPK)-3 and MAPK-1, also known as extracellular signal regulated kinases 1 and 2 (ERK1/2), are phosphorylated and activated during meiotic maturation and inactivated after fertilization. This time frame is similar to the BTG4 accumulation followed by bulk degradation of maternal mRNA (**Fig. 6b**). Therefore, we investigated the potential involvement of ERK1/2 in regulating *Btg4*-mRNA translation during meiotic maturation. U0126, an inhibitor of ERK1/2 activation, blocked the accumulation of BTG4 during oocyte meiotic maturation (**Fig. 7a**), the translation of injected FLAG-GFP–*Btg4* 3′-UTR mRNA (**Fig. 7b**,**c**) and the addition of a

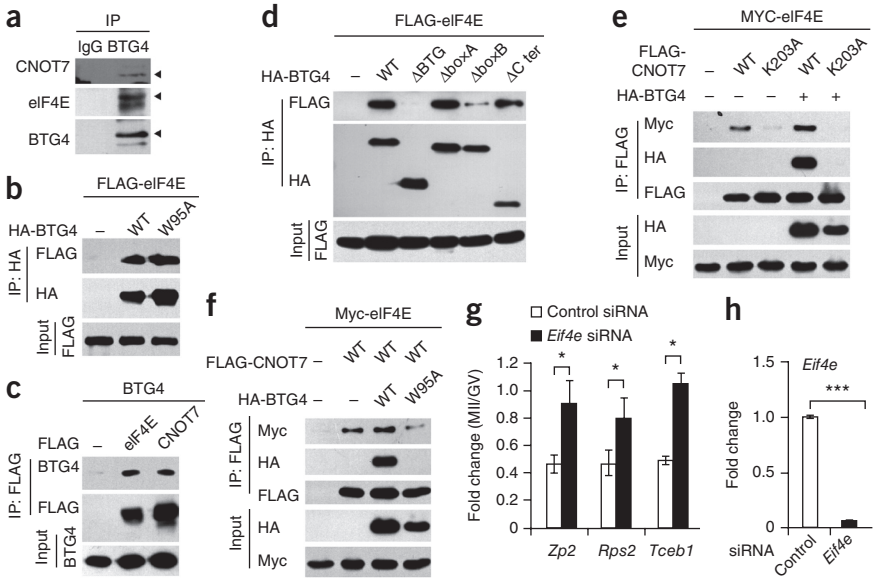

Figure 5 BTG4 is an adaptor protein that mediates the interaction between CNOT7 and eIF4E. Uncropped images of western blots are in **Supplementary Data Set 1**. (**a**) Western blot of Co-IP assay showing BTG4 interactions with CNOT7 and eIF4E in mature oocytes. (**b**) Co-IP results showing the interactions of WT and W95-mutated BTG4 with eIF4E. (**c**) Protein pulldown assay showing the interaction of purified BTG4 with eIF4E and CNOT7 *in vitro*. (**d**) Domain-mapping results showing interactions of BTG4 mutants with eIF4E. (**e**) Co-IP assay showing the interactions of CNOT7 and the CNOT7 K203A mutant with eIF4E. C ter, C terminus. (**f**) Co-IP assay showing the CNOT7-eIF4E interaction with the overexpression of BTG4 and the BTG4 W95A mutant. (**g**) qRT–PCR results showing levels of indicated maternal transcripts in oocytes without or with eIF4E RNA interference. $n = 3$ technical replicates. Error bars, s.e.m. $^{*}P < 0.05$ by two-tailed Student's *t* test. (**h**) qRT–PCR results showing the efficiency of *Eif4e* RNA interference in oocytes at the GV stage. $n = 3$ technical replicates. Error bars, s.e.m. $^{***}P < 0.001$ by two-tailed Student's *t* test.

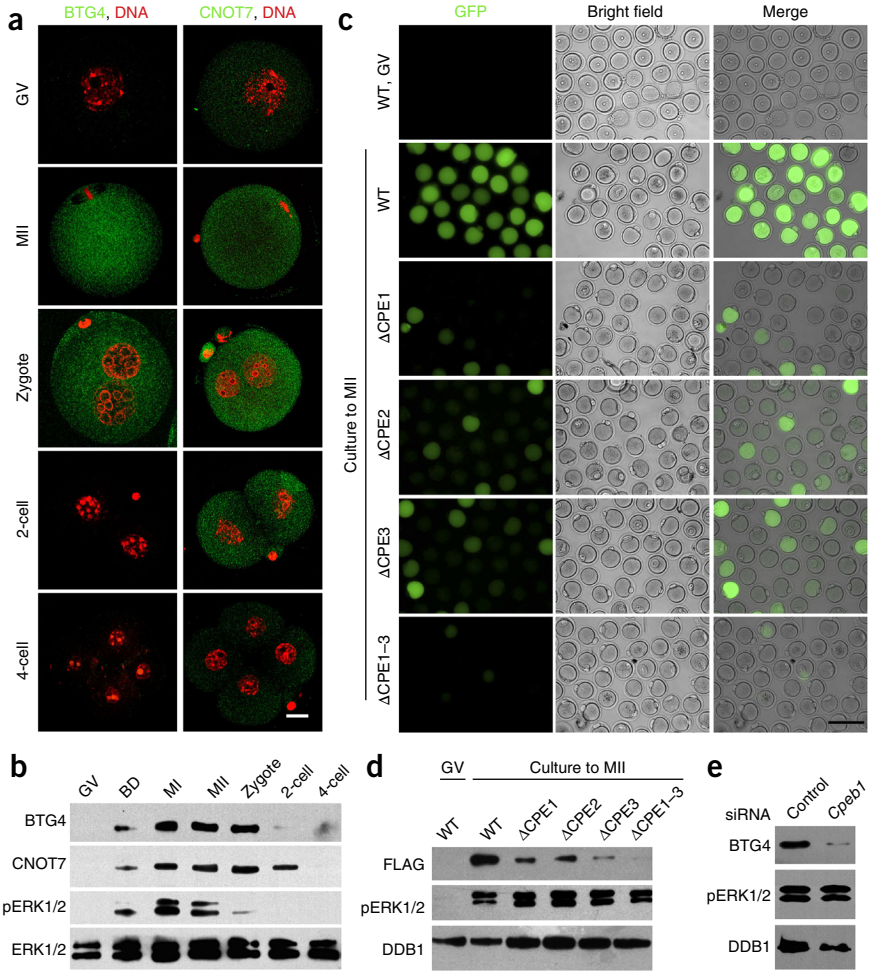

Figure 6 *Btg4*-mRNA translation is coupled to the meiotic cell cycle by its 3′ UTR. (**a**) Immunofluorescence showing expression and distribution of BTG4 and CNOT7 in mouse oocytes and early embryos. Scale bar, 10 µm. (**b**) Protein levels of BTG4, CNOT7, and phosphorylated ERK1/2 (pERK1/2) in oocytes and embryos at the indicated stages. (**c**,**d**) Fluorescence microscopy (**c**) and western blotting (**d**) results showing meiotic maturation- and CPE-dependent activation of the *Btg4* 3′ UTR. Scale bar, 100 µm. (**e**) Protein levels of BTG4 in oocytes injected with control and cytoplasmic polyadenylation element binding protein-1 (*Cpeb1*) short interfering RNA (siRNA). Uncropped images of western blots are in **Supplementary Data Set 1**.

poly(A)-tail to *Btg4* mRNA at MI (**Fig. 7d**). To further investigate the regulation of BTG4 by ERK1/2 *in vivo*, we selectively deleted *Erk1* (official symbol *Mapk3*) and *Erk2* (official symbol *Mapk1*) in the oocytes (denoted *Erk1/2*$^{oo-/-}$). BTG4 protein remained undetectable at the MII stage (**Fig. 7e**). However, ERK1/2 phosphorylation was not blocked in mature *Btg4*$^{-/-}$ or *Btg4*$^{W95A/-}$ oocytes (**Figs. 1c** and **4b**), thus indicating that BTG4 is downstream of ERK1/2. Collectively, these results indicate that ERK1/2 activity is the key signal that couples *Btg4*-mRNA translation to meiotic cell-cycle progression.

DISCUSSION

In this study, we identified *Btg4* as a new maternal-effect gene that functions as an MZT licensing factor in mammals, and we found that accumulation of BTG4 protein in maturing oocytes creates a time frame for CCR4–NOT deadenylase–mediated decay of maternal mRNA (**Fig. 8**). BTG4 belongs to the BTG and TOB family, which includes six members (BTG1–4, TOB1 and TOB2) in vertebrates[14]. Knockout mice have been reported for all BTG and TOB family members except for *Btg4* (**Supplementary Table 4**). None of these mice show appreciable phenotypes, thus suggesting that BTG- and TOB-encoding genes play redundant roles. Only *Btg4* is indispensable and exclusively expressed in oocytes. However, *fog-3*, the sole BTG- or TOB-encoding gene in *Caenorhabditis elegans*, is a key regulator of germ-cell development[35]. The only defect observed in *fog-3* mutants is sexual transformation of the germline[36]. Our study indicates that the regulation of animal reproduction by BTG- and TOB-encoding genes has been conserved in evolution, although detailed scenarios vary among species to accommodate different developmental strategies. It also demonstrates that *Btg4* is an MZT licensing factor in mammalian oocytes.

BTG and TOB proteins inhibit proliferation in cultured cells by interacting with CNOT7 and CNOT8 (ref. 22). However, the underlying biochemical mechanism has not been clarified. TOB1 and TOB2 have conserved PAM2 domains in the C-terminal region, which bind poly(A)-binding proteins and recruit CNOT7 and CNOT8 to

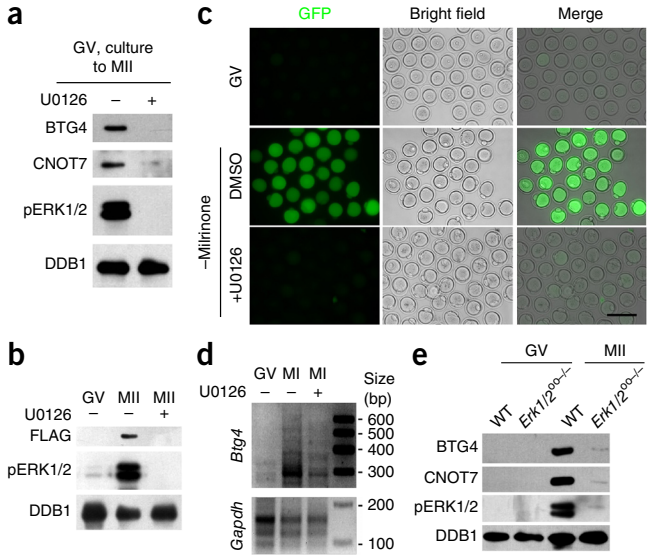

Figure 7 ERK1/2 triggers *Btg4*-mRNA translation by targeting its 3′ UTR. (**a**) Western blot results showing levels of phosphorylated ERK1/2 as well as BTG4 and CNOT7 expression in MII oocytes with or without U0126 treatment. (**b**,**c**) Western blot (**b**) and epifluorescence (**c**) showing the expression of FLAG-GFP fused with the *Btg4* 3′ UTR in MII oocytes with or without U0126 treatment, in the absence of milrinone. Scale bar, 100 µm. (**d**) PAT assay results showing the poly(A)-tail addition to *Btg4* mRNA in MI oocytes with or without U0126 treatment. (**e**) Protein levels of BTG4, CNOT7, and phospho-ERK1/2 in oocytes of WT and *Erk1/2*$^{oo-/-}$ mice at GV and MII stages. Uncropped images of western blots are in **Supplementary Data Set 1**.

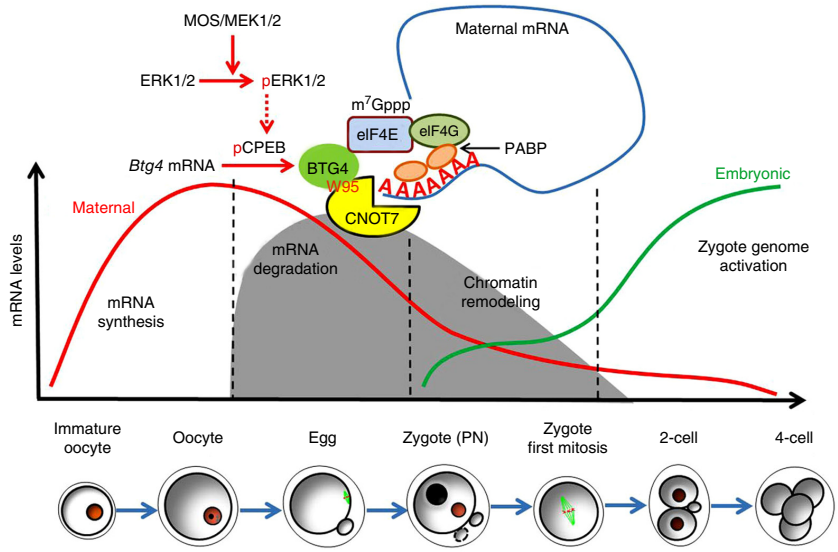

Figure 8 Summary of BTG4 function and regulation during MZT. *Btg4* mRNAs are stored in fully grown oocytes. During meiotic resumption, the ERK1/2 cascade and CPEB1 are sequentially activated. CPEB1 stimulates polyadenylation and translation of *Btg4* mRNA by interacting with three CPEs in its 3′ UTR. In maturing oocytes, BTG4 proteins mediate the interaction between CNOT7 or CNOT8 and eIF4E, and recruit the CCR4–NOT deadenylases to the translating maternal transcripts. As a result, maternal transcripts are degraded during oocyte maturation and fertilization. This event is a prerequisite for zygotic genome activation. Red and green curves represent maternal and zygotic transcripts, respectively. The gray shaded area represents the time frame of BTG4 protein expression. MOS/MEK1/2 indicates the MOS–mitogen-activated protein kinase kinase 1 and 2 cascade. PABP, poly(A)-binding protein; PN, pronucleus.

poly(A) tails[37]. However, the C-terminal regions of BTG proteins are short and lack PAM2 domains. Instead, BTG proteins mediate the interaction between the translation initiation factor eIF4E and CNOT7 in oocytes and cultured cells. The actively translating mRNAs are closed loops in which the 5′-cap-bound translation initiation complex (containing eIF4E) interacts with 3′-poly(A)-tail-bound poly(A)-binding proteins[38]. Therefore, BTG4 might function as an adaptor protein that specifically recruits the CCR4–NOT deadenylase to the loop junction in oocytes and zygotes, and triggers mRNA decay. Depletion of eIF4E in oocytes also impaired decay of maternal mRNA, thus further suggesting that BTG4-eIF4E binding is important for the recognition of translating mRNAs by the CCR4–NOT deadenylase. Further studies are required to confirm whether eIF4E is a linker molecule that couples the sequential biochemical processes of protein translation and mRNA degradation. Beyond its function in triggering mRNA translation, eIF4E may also serve as a docking molecule for the CCR4–NOT deadenylase, particularly during MZT. Under the same mechanism, BTG proteins might destabilize translating messenger ribonucleoprotein particles in cultured somatic cells and inhibit cell proliferation.

Btg4 and *Cnot7* mRNAs are exclusively expressed in fully grown oocytes but are translated into proteins only after meiotic resumption, thus facilitating CCR4–NOT–mediated mRNA decay. This observation addresses the long-standing question of the factors that trigger mRNA destabilization during MZT. Furthermore, CNOT7 is normally expressed in *Btg4*$^{-/-}$ and *Btg4*$^{W95A/-}$ oocytes but does not trigger poly(A) shortening of its target transcripts without this adaptor protein, thus indicating that BTG4 is a rate-limiting or licensing factor of CCR4–NOT deadenylase activity in oocytes. Several meiosis-associated genes (including *Dazl*, *Mos*, and *Ccnb1*) are regulated by poly(A)-tail addition during meiosis, as mediated by the interaction of CPE and CPEBs[39,40]. Our study provides evidence for the inclusion of *Btg4* in this category. However, unlike the aurora A–stimulated CPEB1 activation and poly(A) elongation in *Xenopus* oocytes[32], translation of BTG4 and CNOT7 is stringently coupled with progression of the meiotic cell cycle through intraoocyte activation of the MAPK cascade. ERK1/2 inhibition or deletion in oocytes blocked BTG4 and CNOT7 translation, and stabilized a subset of maternal mRNAs in mature oocytes and zygotes. Here we demonstrate a previously unrealized role for ERK1/2 as a pace-keeper of MZT, beyond its well-recognized function in spindle assembly and MII-arrest maintenance (**Fig. 8**).

However, not all mRNA-degradation events during MZT are BTG4 dependent. RNA-seq results indicated that only a subset of maternal mRNAs were stabilized in *Btg4*-knockout oocytes. Other deadenylases, such as the PAN2–PAN3 complex, which has been shown to cooperate with CCR4–NOT, may also be involved in decay of maternal mRNA during MZT[41,42]. In addition, because MZT in mammalian embryos takes place at very early stages of development (two- to four-cell stage), degradation of maternal mRNA may completely rely on these oocyte factors, without any contribution of zygotic factors. Our study elucidated that ERK1/2-triggered *Btg4*-mRNA translation is a key step in oocyte cytoplasmic maturation and revealed that decay of maternal mRNA, as mediated by BTG4–CNOT7 and BTG4–CNOT8, is required for successful ZGA, which determines the developmental potential of embryos.

METHODS

Methods and any associated references are available in the online version of the paper.

Accession codes. RNA-seq data have been deposited in the NCBI Gene Expression Omnibus database under accession code GSE71257.

Note: Any Supplementary Information and Source Data files are available in the online version of the paper.

ACKNOWLEDGMENTS

This study was funded by the National Basic Research Program of China (2012CB944403) and the National Natural Science Foundation of China (31528016, 91519313, and 31371449) to H.-Y.F. We thank B. Zhang (Peking University) for vectors.

AUTHOR CONTRIBUTIONS

H.-Y.F. and C.Y. conceived the project. H.-Y.F., C.Y., S.-Y.J., Q.-Q.S., Y.D., Y.-L.Z., and F.T. designed and analyzed experiments. C.Y., S.-Y.J., Q.-Q.S., Y.D., Y.-L.Z., J.-J.Z., Y.L., B.H., and S.-C.S. performed experiments. Z.-W.W. and Q.-Y.S. assisted in microinjection of mouse embryos. C.Y., Y.-L.Z., and H.-Y.F. wrote the paper. C.Y., S.-Y.J., Q.-Q.S., Y.D., J.-J.Z., and Y.-L.Z. contributed equally to this work.

COMPETING FINANCIAL INTERESTS

The authors declare no competing financial interests.

1. Schier, A.F. The maternal-zygotic transition: death and birth of RNAs. *Science* **316**, 406–407 (2007).

2. Li, L., Lu, X. & Dean, J. The maternal to zygotic transition in mammals. *Mol. Aspects Med.* **34**, 919–938 (2013).
3. Schultz, R.M. From egg to embryo: a peripatetic journey. *Reproduction* **130**, 825–828 (2005).
4. Li, L., Baibakov, B. & Dean, J. A subcortical maternal complex essential for preimplantation mouse embryogenesis. *Dev. Cell* **15**, 416–425 (2008).
5. Christians, E., Davis, A.A., Thomas, S.D. & Benjamin, I.J. Maternal effect of *Hsf1* on reproductive success. *Nature* **407**, 693–694 (2000).
6. Burns, K.H. *et al.* Roles of NPM2 in chromatin and nucleolar organization in oocytes and embryos. *Science* **300**, 633–636 (2003).
7. Wu, X. *et al.* Zygote arrest 1 (*Zar1*) is a novel maternal-effect gene critical for the oocyte-to-embryo transition. *Nat. Genet.* **33**, 187–191 (2003).
8. Walser, C.B. & Lipshitz, H.D. Transcript clearance during the maternal-to-zygotic transition. *Curr. Opin. Genet. Dev.* **21**, 431–443 (2011).
9. Schellander, K., Hoelker, M. & Tesfaye, D. Selective degradation of transcripts in mammalian oocytes and embryos. *Theriogenology* **68** (Suppl. 1), S107–S115 (2007).
10. Hou, Y. *et al.* Genome analyses of single human oocytes. *Cell* **155**, 1492–1506 (2013).
11. Gallardo, T.D. *et al.* Genomewide discovery and classification of candidate ovarian fertility genes in the mouse. *Genetics* **177**, 179–194 (2007).
12. Qiu, Z. *et al.* High-efficiency and heritable gene targeting in mouse by transcription activator-like effector nucleases. *Nucleic Acids Res.* **41**, e120 (2013).
13. Huang, P. *et al.* Heritable gene targeting in zebrafish using customized TALENs. *Nat. Biotechnol.* **29**, 699–700 (2011).
14. Winkler, G.S. The mammalian anti-proliferative BTG/Tob protein family. *J. Cell. Physiol.* **222**, 66–72 (2010).
15. Tirone, F. The gene PC3(TIS21/BTG2), prototype member of the PC3/BTG/TOB family: regulator in control of cell growth, differentiation, and DNA repair? *J. Cell. Physiol.* **187**, 155–165 (2001).
16. Cong, L. *et al.* Multiplex genome engineering using CRISPR/Cas systems. *Science* **339**, 819–823 (2013).
17. Wang, H. *et al.* One-step generation of mice carrying mutations in multiple genes by CRISPR/Cas-mediated genome engineering. *Cell* **153**, 910–918 (2013).
18. Charlesworth, A., Meijer, H.A. & de Moor, C.H. Specificity factors in cytoplasmic polyadenylation. *Wiley Interdiscip. Rev. RNA* **4**, 437–461 (2013).
19. Buanne, P. *et al.* Cloning of PC3B, a novel member of the PC3/BTG/TOB family of growth inhibitory genes, highly expressed in the olfactory epithelium. *Genomics* **68**, 253–263 (2000).
20. Mauxion, F., Chen, C.Y., Séraphin, B. & Shyu, A.B. BTG/TOB factors impact deadenylases. *Trends Biochem. Sci.* **34**, 640–647 (2009).
21. Doidge, R., Mittal, S., Aslam, A. & Winkler, G.S. Deadenylation of cytoplasmic mRNA by the mammalian Ccr4-Not complex. *Biochem. Soc. Trans.* **40**, 896–901 (2012).
22. Doidge, R., Mittal, S., Aslam, A. & Winkler, G.S. The anti-proliferative activity of BTG/TOB proteins is mediated via the Caf1a (CNOT7) and Caf1b (CNOT8) deadenylase subunits of the Ccr4-not complex. *PLoS One* **7**, e51331 (2012).
23. Miller, J.E. & Reese, J.C. Ccr4-Not complex: the control freak of eukaryotic cells. *Crit. Rev. Biochem. Mol. Biol.* **47**, 315–333 (2012).
24. Horiuchi, M. *et al.* Structural basis for the antiproliferative activity of the Tob-hCaf1 complex. *J. Biol. Chem.* **284**, 13244–13255 (2009).
25. Winkler, G.S. & Balacco, D.L. Heterogeneity and complexity within the nuclease module of the Ccr4-Not complex. *Front. Genet.* **4**, 296 (2013).
26. Gosselin, P. *et al.* Tracking a refined eIF4E-binding motif reveals Angel1 as a new partner of eIF4E. *Nucleic Acids Res.* **41**, 7783–7792 (2013).
27. Matsuo, H. *et al.* Structure of translation factor eIF4E bound to m7GDP and interaction with 4E-binding protein. *Nat. Struct. Biol.* **4**, 717–724 (1997).
28. Marcotrigiano, J., Gingras, A.C., Sonenberg, N. & Burley, S.K. Cocrystal structure of the messenger RNA 5′ cap-binding protein (eIF4E) bound to 7-methyl-GDP. *Cell* **89**, 951–961 (1997).
29. Ptushkina, M. *et al.* Cooperative modulation by eIF4G of eIF4E-binding to the mRNA 5′ cap in yeast involves a site partially shared by p20. *EMBO J.* **17**, 4798–4808 (1998).
30. Sarkissian, M., Mendez, R. & Richter, J.D. Progesterone and insulin stimulation of CPEB-dependent polyadenylation is regulated by Aurora A and glycogen synthase kinase-3. *Genes Dev.* **18**, 48–61 (2004).
31. Richter, J.D. Breaking the code of polyadenylation-induced translation. *Cell* **132**, 335–337 (2008).
32. Mendez, R. *et al.* Phosphorylation of CPE binding factor by Eg2 regulates translation of *c-mos* mRNA. *Nature* **404**, 302–307 (2000).
33. Groisman, I. *et al.* CPEB, maskin, and cyclin B1 mRNA at the mitotic apparatus: implications for local translational control of cell division. *Cell* **103**, 435–447 (2000).
34. Eliscovich, C., Peset, I., Vernos, I. & Méndez, R. Spindle-localized CPE-mediated translation controls meiotic chromosome segregation. *Nat. Cell Biol.* **10**, 858–865 (2008).
35. Ellis, R.E. & Kimble, J. The fog-3 gene and regulation of cell fate in the germ line of *Caenorhabditis elegans*. *Genetics* **139**, 561–577 (1995).
36. Chen, P.J., Cho, S., Jin, S.W. & Ellis, R.E. Specification of germ cell fates by FOG-3 has been conserved during nematode evolution. *Genetics* **158**, 1513–1525 (2001).
37. Ezzeddine, N. *et al.* Human TOB, an antiproliferative transcription factor, is a poly(A)-binding protein-dependent positive regulator of cytoplasmic mRNA deadenylation. *Mol. Cell. Biol.* **27**, 7791–7801 (2007).
38. Richter, J.D. & Lasko, P. Translational control in oocyte development. *Cold Spring Harb. Perspect. Biol.* **3**, a002758 (2011).
39. Piqué, M., López, J.M., Foissac, S., Guigó, R. & Méndez, R. A combinatorial code for CPE-mediated translational control. *Cell* **132**, 434–448 (2008).
40. Chen, J. *et al.* Genome-wide analysis of translation reveals a critical role for deleted in azoospermia-like (Dazl) at the oocyte-to-zygote transition. *Genes Dev.* **25**, 755–766 (2011).
41. Wolf, J. *et al.* Structural basis for Pan3 binding to Pan2 and its function in mRNA recruitment and deadenylation. *EMBO J.* **33**, 1514–1526 (2014).
42. Zheng, D. *et al.* Deadenylation is prerequisite for P-body formation and mRNA decay in mammalian cells. *J. Cell Biol.* **182**, 89–101 (2008).

ONLINE METHODS

Mice. Wild type ICR-strain mice were obtained from the Zhejiang Academy of Medical Science, China. Mice were maintained under SPF conditions in a controlled environment of 20–22 °C, with a 12 h–12 h light–dark cycle, 50–70% humidity, and food and water provided *ad libitum*. Animal care and experimental procedures were conducted in accordance with the Animal Research Committee guidelines of Zhejiang University. *Erk1*$^{-/-}$, *Erk2*$^{flox/flox}$, and *Gdf9-Cre* mice were as previously reported[43,44]. All mutant mouse strains had an ICR background. The experiments were randomized and were performed with blinding to the conditions of the experiments. No statistical method was used to predetermine sample size. Genotyping primers used are listed in **Supplementary Table 2**.

Construction of transcription activator-like effector nuclease (TALEN) expression vectors targeting mouse *Btg4*. A target site was identified with the online software published by Cermak *et al.* (https://tale-nt.cac.cornell.edu/node/add/talen-old/). Nucleotide-recognizing TALE single-unit vectors and TALEN expression vectors were kind gifts from B. Zhang (Peking University). TALE repeat arrays and TALE nuclease expression vectors were constructed as previously described[13]. The expected nucleotide-deletion site contained an endogenous ScaI restriction site. This feature was used for detection of *Btg4*-mutated founder mice.

***In vitro* transcription and preparation of mRNAs for microinjections.** To prepare mRNAs for microinjection, expression vectors were linearized and subjected to phenol–chloroform extraction and ethanol precipitation. The linearized DNAs were transcribed with a SP6 mMESSAGE mMACHINE Kit (Invitrogen, AM1450) per the manufacturer's instructions. mRNAs were recovered by lithium chloride precipitation and resuspended in nuclease-free water.

Production of *Cas9* mRNA, sgRNAs, and donor oligos for *Btg4*^{W95A} knock-in. The codon-optimized CAS9 expression construct, CAS9-N-NLS-FLAG-linker (Addgene, 44758), was synthesized and inserted into a pST1374 vector as previously described[45]. The pUC57-sgRNA expression vector used for *in vitro* transcription of sgRNAs was as previously described[46]. Oligos for the generation of mouse *Btg4*^{W95}-targeting sgRNA expression plasmids (**Supplementary Table 2**) were annealed and cloned into the BsaI sites of pUC57-sgRNA.

In vitro transcription was performed as previously described[46]. Briefly, the pST1374-CAS9-N-NLS-FLAG-linker vector was linearized with the AgeI enzyme and *in vitro* transcribed with a T7 Ultra Kit (Ambion, AM1345). CAS9-NNLS-FLAG-linker mRNA was purified with an RNeasy Mini Kit (Qiagen, 74104). sgRNA oligos were annealed into a pUC57-sgRNA expression vector with a T7 promoter. Then, expression vectors were linearized by DraI and transcribed *in vitro* with a MEGAshortscript kit (Ambion, AM1354). sgRNAs were purified with a MEGAclear Kit (Ambion, AM1908) and recovered by alcohol precipitation.

A single-stranded oligo with 60-bp homology to sequences on each side surrounding m*Btg4*^{W95} was ordered as ultramer DNA oligos from Integrated DNA Technologies (IDT). The oligo contained a TG-to-GC mutation, which changed the W95 to alanine and destroyed an endogenous NdeI restriction site. This feature was used for detection of m*Btg4*^{W95} mutations.

Microinjection of oocytes and zygotes. For microinjection, fully grown GV oocytes were harvested in M2 medium with 2 μM milrinone to inhibit spontaneous GV breakdown. All injections were performed with an Eppendorf Transferman NK2 micromanipulator. Denuded oocytes were injected with 5- to 10-pL samples per oocyte. After injection, oocytes were washed and cultured in M2 medium plus 2 μM milrinone at 37 °C with 5% CO_2.

Mouse zygotes were obtained by superovulation of 7- to 8-week-old females mated with males of the same strain. For *Btg4* knockout, 40 ng/μl mRNA of each TALEN pair was injected into the cytoplasm of zygotes with well-recognized pronuclei, in M2 medium (Sigma). For *Btg4*^{W95A} knock-in, *Cas9* mRNA (100 ng/ml), sgRNA (50 ng/ml), and donor oligos (100 ng/ml) were mixed and injected. Injected zygotes were transferred into pseudopregnant ICR female mice (15–25 zygotes per mouse) after 2 h recovery culture in KSOM medium.

Founder identification, TA cloning, and sequencing. Tail clips were subjected to standard DNA-extraction procedures. For identification of *Btg4*-mutated founders, the extracted DNA was amplified with GT-F and GT-R primers (**Supplementary Table 2**) flanking the target sites, which generated products of 683 bp. The amplified DNA fragments were digested with ScaI, and those resistant to ScaI digestion were subjected to TA cloning and sequencing.

For identification of *Btg4*^{W95A} knock-in founders, the extracted DNA was amplified with the W95-F and W95-R primers (**Supplementary Table 2**) flanking the *Btg4*^{W95A} sites, which generated products of 894 bp. The amplified DNA fragments were digested with NdeI, and those resistant to NdeI digestion were subjected to TA cloning and sequencing.

To identify exact genomic DNA modifications in founders, PCR products from each mutated founder were cloned with a TA cloning kit (Takara) according to the manufacturer's instructions. At least six colonies were picked from each transformation and sequenced.

The founder mice were crossed to WT mice for three generations to avoid potential off-target effects due to TALEN-mediated DNA editing. The *Btg4*-null allele and *Btg4*^{W95A} allele were effectively passed between generations.

Superovulation and fertilization. For superovulation, female mice (21–23 days old) were intraperitoneally injected with 5 IU of pregnant mare's serum gonadotropin (PMSG, Ningbo Sansheng Pharmaceutical). After 44 h, mice were then injected with 5 IU of human chorionic gonadotropin (hCG, Ningbo Sansheng Pharmaceutical). After an additional 16 h, oocyte-cumulus masses were surgically removed from the oviducts, and the numbers of oocytes were counted after digestion with 0.3% hyaluronidase (Sigma-Aldrich). Oocyte morphology was observed, and images were acquired with a Nikon SMZ1500 stereoscope.

To obtain early embryos, female mice were mated with 10- to 12-week-old WT males. Successful mating was confirmed by the presence of vaginal plugs. Embryos were harvested from oviducts at the indicated times after hCG injection.

Confocal microscopy for mouse oocytes and embryos. Oocytes and embryos were fixed in PBS-buffered 4% paraformaldehyde (PFA) for 30 min at room temperature, and this was followed by permeabilization with 0.2% Triton X-100. After being blocked with 1% BSA in PBS, oocytes were incubated with primary antibodies diluted in blocking solution at room temperature for 1 h. After being washed three times with PBS, oocytes were labeled with secondary antibodies for 45 min, and then counterstained with 5 μg/ml of 4′,6-diamidino-2-phenylindole (DAPI) or propidium iodide (PI) (Molecular Probes, Life Technologies) for 10 min. Oocytes were mounted on glass slides with SlowFade Gold Antifade Reagent (Life Technologies) and examined under a confocal laser scanning microscope (Zeiss LSM 710, Carl Zeiss).

Oocyte and embryo culture. Mice at 21 days of age were injected with 5 IU of PMSG and were humanely euthanized 44 h later. Oocytes at the GV stage were harvested in M2 medium (M7167; Sigma-Aldrich) and cultured in minidrops of M16 medium (M7292; Sigma-Aldrich) covered with mineral oil (M5310; Sigma-Aldrich) at 37 °C in a 5% CO_2 atmosphere. Zygotes were harvested from fertilized females 24 h after the hCG injection and cultured in KSOM medium (Millipore).

Histological analysis and immunohistochemistry. Ovary samples fixed in PBS-buffered formalin and embedded in paraffin were sectioned (5 μm thick) for hematoxylin and eosin (HE) staining and immunohistochemistry (IHC). For IHC, sections were deparaffinized and rehydrated. Primary antibodies were applied at suitable dilutions (**Supplementary Table 3**) at room temperature for 1 h, and samples were then incubated with biotinylated secondary antibodies for 30 min. Sections were then stained with Vectastain ABC and DAB peroxidase substrate kits (Vector Laboratories). Antibodies used in this study are listed in **Supplementary Table 3**.

Western blot analysis. Oocytes were lysed with SDS sample buffer (200 oocytes per sample) and heated for 5 min at 95 °C. Total oocyte proteins were separated by SDS-PAGE and electrophoretically transferred to PVDF membranes (Millipore); this was followed by blocking in TBST containing 5% defatted milk (BD) for 30 min. After being probed with primary antibodies, the membranes were washed in TBST, incubated with an HRP-linked secondary antibody (Jackson ImmunoResearch Laboratories) for 1 h, and washed three times with TBST. Bound antibodies were detected with Super Signal West Femto maximum sensitivity substrate (Thermo Fisher). The primary antibodies and dilution

factors used are listed in **Supplementary Table 3**. The western blots are presented in uncropped form with molecular weight markers in **Supplementary Data Set 1**.

Cell culture, plasmid transfection, and immunoprecipitation. HeLa cells and HEK293 cells were from the American Type Culture Collection and were grown in DMEM (Invitrogen) supplemented with 10% FBS (Hyclone) and 1% penicillin–streptomycin solution (Gibco) at 37 °C in a humidified 5% CO_2 incubator. Cell lines were in healthy condition but were not tested for mycoplasma contamination.

Mouse *Btg4*, *Btg2*, *Btg3*, *Cnot7*, and *Cnot8* cDNAs were PCR-amplified from a mouse ovarian cDNA pool and cloned into pCS2- or pcDNA-based eukaryotic expression vectors. Transient plasmid transfection was performed with Lipofectamine 2000 (Invitrogen).

After a 48-h transfection, cells were lysed in lysis buffer (50 mM Tris-HCl, pH 7.5, 150 mM NaCl, 10% glycerol, and 0.5% NP-40, with protease and phosphatase inhibitors added before use.). After centrifugation at 12,000*g* for 10 min, the supernatant was subjected to immunoprecipitation with different affinity gels (Sigma). After incubation at 4 °C for 4 h, beads were washed three times with lysis buffer. SDS sample buffer was added to the beads, and the eluates were used for western blot analysis.

Poly(A)-tail (PAT) assay. Total RNA was isolated from oocytes at the indicated stages with an RNeasy Mini kit (Qiagen). The RNA was then hybridized with or without oligo$(dT)_{20}$ before RNase H treatment. RNA was purified and ligated with the anchor primer P1 (5′-P-GGTCACCTTGATCTGAAGC-NH_2-3′) for 1 h at 37 °C with T4 RNA ligase (New England BioLabs). Reverse transcription was performed with a SuperScript III kit (Invitrogen) with the P1-antisense primer P2 (5′-GCTTCAGATCAAG GTGACCTTTTT-3′). The products were used in a PCR reaction with gene-specific primers (**Supplementary Table 2**) under the following conditions: 30 s at 94 °C, 60 s at 56 °C, and 60 s at 72 °C. PCR products were analyzed on a 2.5% agarose gel.

Deadenylation assay. HEK293 cells were transfected with plasmids encoding FLAG-tagged CNOT7 with or without HA-tagged BTG4 or its W95A mutation. After 48 h, the cells were lysed in lysis buffer (50 mM Tris-HCl, pH 7.5, 150 mM NaCl, 5 mM MgCl2, 0.5 mM EDTA, 5% glycerol, 1 mM dithiothreitol, and protease inhibitors). FLAG-CNOT7 proteins were immunoprecipitated with anti-FLAG M2 affinity gel (Sigma) and eluted with 0.3 mg/ml triple-FLAG peptides in deadenylase buffer (50 mM HEPES-NaOH, pH 8.0, 150 mM NaCl, 2 mM $MgCl_2$, 10% glycerol, 1 mM DTT, and protease inhibitors) by peptide competition. Subsequently, 1 µl 5′-Cy5.5-labeled substrate (Sigma, Cy5.5-5′-UCUAAAU AAAAAAAAAAAAAAAAAAA-3′; final concentration, 0.1 µM) was added to 9.0 µl FLAG eluate and incubated for 60 min at 37 °C. Reactions were stopped by the addition of 12 µl RNA loading buffer (95% formamide, 0.025% bromophenol blue, 0.025% xylene cyanol FF, 0.025% SDS, and 5 mM EDTA) and heated for 3 min at 85 °C. The RNA was analyzed by 25% denaturing PAGE containing 8.3 M urea. Cy5.5-labeled RNA was visualized with an Odyssey imager (680 nm).

RNA isolation and library construction. GV oocytes, MII oocytes, zygotes, and two-cell embryos were collected from WT and *Btg4*$^{-/-}$ or *Erk1/2*$^{oo-/-}$ mice (60 per sample). Total RNA was extracted from each sample with an RNeasy Plus Micro kit (Qiagen) according to the manufacturer's protocol. In the initial step, we spiked 2×10^6 mRNA-GFP and 2×10^6 mRNA-RFP, transcribed *in vitro*, into each lysed sample for RNA isolation. Extracted total RNA was used to prepare a sequencing library with an NEB Next Ultra RNA Library Prep Kit for Illumina. Briefly, mRNA was purified with oligo$(dT)_{25}$ beads, fragmented, and then reverse transcribed. The second strand was then synthesized with random primers in succession. Afterward, double-stranded cDNA was subjected to end repair, A-tailing, adaptor ligation, and PCR amplification of 12–14 cycles to obtain the library.

RNA-seq data analysis. We aligned RNA-seq reads, sequenced with an Illumina HiSeq 2500, to *Mus musculus* UCSCmm9 references with TopHat (http://ccb.jhu.edu/software/tophat/index.shtml) and calculated the FPKM of each gene with Cufflinks (http://cole-trapnell-lab.github.io/cufflinks/). The amount of total mRNA was calculated on the basis of the FPKM of exogenous GFP and RFP. The expression level of each gene was calculated as its FPKM normalized to the FPKM of GFP/RFP. Differentially expressed genes (DEGs) were assessed with the DESeq2 package at a P value of <0.05, false discovery rate (FDR) of <0.05 and fold change (FC) of >2 or <0.5 (ref. 47). The RNA-seq data in this work have been deposited in the NCBI Gene Expression Omnibus (GEO) under accession number GSE71257.

RNA isolation and real-time RT–PCR. Total RNA was extracted with an RNeasy Mini kit (Qiagen) according to the manufacturer's instructions. Real-time RT–PCR analysis was performed with a Power SYBR Green PCR Master Mix (Applied Biosystems, Life technologies) and an Applied Biosystems 7500 Real-Time PCR System. Relative mRNA levels were calculated by normalizing to the levels of endogenous β-actin mRNA (internal control) with Microsoft Excel. The relative transcript levels of samples were compared with those of the control, and the fold changes are reported. For each experiment, qPCR reactions were performed in triplicate. Primer sequences are listed in **Supplementary Table 2**.

Statistical analysis. Results are reported as means ± s.e.m. Each experiment included at least three independent samples and was repeated at least three times. Results for two experimental groups were compared by two-tailed unpaired Student's t tests. Statistically significant values of P <0.05, P <0.01, and P <0.001 are indicated by one, two, and three asterisks, respectively.

43. Fan, H.Y. *et al.* MAPK3/1 (ERK1/2) in ovarian granulosa cells are essential for female fertility. *Science* **324**, 938–941 (2009).
44. Lan, Z.J., Xu, X. & Cooney, A.J. Differential oocyte-specific expression of Cre recombinase activity in GDF-9-iCre, Zp3cre, and Msx2Cre transgenic mice. *Biol. Reprod.* **71**, 1469–1474 (2004).
45. Shen, B. *et al.* Generation of gene-modified mice via Cas9/RNA-mediated gene targeting. *Cell Res.* **23**, 720–723 (2013).
46. Zhou, J. *et al.* One-step generation of different immunodeficient mice with multiple gene modifications by CRISPR/Cas9 mediated genome engineering. *Int. J. Biochem. Cell Biol.* **46**, 49–55 (2014).
47. Love, M.I., Huber, W. & Anders, S. Moderated estimation of fold change and dispersion for RNA-seq data with DESeq2. *Genome Biol.* **15**, 550 (2014).

doi:10.1038/nsmb.3204